APR 2 1 2006

REPORT DOCUMENTATION PAGE

Form Approved
OMB No. 0704-0188

1. AGENCY USE ONLY *(Leave blank)*	2. REPORT DATE	3. REPORT TYPE AND DATES COVERED
	14.Apr.06	MAJOR REPORT

4. TITLE AND SUBTITLE
SIZING/OPTIMIZATION OF A SMALL SATELLITE ENERGY STORAGE AND ATTITUDE CONTROL SYSTEM

5. FUNDING NUMBERS

6. AUTHOR(S)
MAJ RICHIE DAVID J

7. PERFORMING ORGANIZATION NAME(S) AND ADDRESS(ES)
UNIVERSITY OF SURREY

8. PERFORMING ORGANIZATION REPORT NUMBER
CI04-1763

9. SPONSORING/MONITORING AGENCY NAME(S) AND ADDRESS(ES)
THE DEPARTMENT OF THE AIR FORCE
AFIT/CIA, BLDG 125
2950 P STREET
WPAFB OH 45433

10. SPONSORING/MONITORING AGENCY REPORT NUMBER

11. SUPPLEMENTARY NOTES

12a. DISTRIBUTION AVAILABILITY STATEMENT
Unlimited distribution
In Accordance With AFI 35-205/AFIT Sup 1

12b. DISTRIBUTION CODE

13. ABSTRACT *(Maximum 200 words)*

14. SUBJECT TERMS

15. NUMBER OF PAGES
10

16. PRICE CODE

17. SECURITY CLASSIFICATION OF REPORT	18. SECURITY CLASSIFICATION OF THIS PAGE	19. SECURITY CLASSIFICATION OF ABSTRACT	20. LIMITATION OF ABSTRACT

Sizing/Optimization of a Small Satellite Energy Storage and Attitude Control System

David J. Richie*, Vaios J. Lappas†, and Phil L. Palmer‡
University of Surrey , Guildford, UK, GU2 7XH§

The recent advent of miniature single gimbal control moment gyroscopes has spawned interest in variable speed versions for combined energy storage and attitude control systems on small satellites. Although much has been studied on the theory behind such a system, little has been done in optimally sizing these actuators for small satellite applications. Therefore, this paper investigates the fundamental design concepts, optimal sizing, and mission benefits for these actuators. Given a set of small satellite agility and energy storage requirements, an optimal, nonlinear programming method is applied to this problem.

Nomenclature

N_{vc}	=	Number of Actuators in VSCMG-suite
$\hat{g}_s, \hat{g}_t, \hat{g}_g$	=	VSCMG Spin, Transverse, and Gimbal axis unit vectors
$\dot{\Omega}$ or $d\Omega$	=	Maximum Wheel Acceleration
$\Omega_{min}, \Omega_{max}$	=	Minimum, Maximum Wheel Speeds
Ω_{struct}	=	Maximum Structural Wheel Speed
$\dot{\delta}, \delta$	=	Gimbal Rate, Gimbal Angle
β	=	CMG Pyramid Angle
χ	=	CMG Torque Efficiency
M_{sc}, M_{ta}	=	Satellite Total Mass, Allowable Mass
N_a, N_r, N_m	=	Attitude Maneuver Required, Actual, Margin Torque
P_a, P_r, P_m	=	Peak Power Available, Demand, and Margin
C_a, C_r, C_m	=	Storage Capacity Available, Required, Margin
M_{a_i}, M_r, M_{m_i}	=	i_{th} Alternative Actual, Allowable, and Margin ACS plus ES Mass
C_{m_b}, P_{m_b}	=	Baseline Capacity, Peak Power Margins
N_{m_b}, M_{m_b}	=	Baseline Torque, Mass Margins
$P_{a_1}, C_{a_1}, M_{a_{1_i}}$	=	Single VSCMG Actual Peak Power, Storage Capacity, and i_{th} Alternative Mass
$P_{m_1}, C_{m_1}, M_{m_{1_i}}$	=	Single VSCMG Peak Power, Storage Capacity, and i_{th} Alternative Mass Design Margins
$m_{rot}(l_{rot})$	=	Wheel Rotor Mass Function
$m_{oth}(l_{rot})$	=	Miscellaneous Mass Function
$m_{kii_{sc}}$	=	CMG Support Structure Mass Scaled by M_{sc}
$m_{dc_{sc}}$	=	DC Wheel Motor Mass Scaled by M_{sc}
$m_b(l_{rot})$	=	Mag. Bearing Mass Function
$m_{m_2}(l_{rot})$	=	Alternative #2 Wheel Motor Mass Function
$m_{m_3}(l_{rot}, \Omega_{max})$	=	Alternative #3 Wheel Motor Mass Function
P_{dens}, E_{dens}	=	Power Density, Energy Density
MS	=	Mass Savings Percentage
N_{wh}	=	Wheel Torque
P_s	=	Wheel Output Shaft Power
c_1, c_2, c_3	=	Equiv Performance, Fixed Parameter Constants
t_f, t_{off}	=	Slew maneuver time, dead-band
r_o, r_i	=	Rotor Outer, Inner Radii
ρ_{rot}	=	Rotor Material Density
l_{rot}	=	Rotor Length
T_e	=	On-orbit Eclipse Duration
k_s	=	Rotor Shape Factor
θ_f	=	Slew maneuver angle
dod	=	Depth of Discharge
h	=	Orbital Altitude
x_{msn}	=	Transmission Efficiency
d_{ty}	=	Eclipse Duty Cycle
V_{bus}	=	Spacecraft Power Bus Voltage
I_{cmg_w}	=	CMG Wheel Spin-axis Inertia
$I_{T_{max}}$	=	Maximal Spacecraft Principal-axis Inertia
I_{w_s}	=	Wheel Spin-axis Inertia
J	=	Optimization Performance Index
σ_θ, σ_r	=	Rotor Radial, Tangential Stress
$\nu_{\theta r}$	=	Rotor Material Poisson's Ratio of Contraction in r-direction Due to Tension in θ-direction
$\nu_{r\theta}$	=	Rotor Material Poisson's Ratio of Contraction in θ-direction Due to Tension in r-direction
E_r, E_θ	=	r-direction, θ-direction Elastic Modulus
α_1, α_2	=	Integration constants in Rotor Stress Equations
λ	=	$(E_\theta/E_r)^{0.5}$
$l_{real}, \dot{\Omega}_{real}$	=	Real World Limits to l_{rot}, $\dot{\Omega}$
t_{sp}, ρ_{sp}	=	Wheel Spoke Thickness, Density
r, Ω	=	Generic Wheel Planar Radius, Angular Speed

1.0 Introduction

Today's small satellites (less than 500 kg in mass) are increasingly considered for large satellite missions such as precision Earth imaging and Space RADAR [1–3]. Difficult hurdles face these small satellites' designers such as meeting stringent mass, power, and volume constraints which significantly impact cost. In order to mitigate costs, the Surrey Space Centre (SSC) in conjunction with Surrey Satellite Technology, Ltd. (SSTL) regularly uses commercial-off-the-shelf (COTS) components in design [1–4]. Another method to reduce cost (by deleting mass) is to combine key satellite functions. For example, a satellite's Energy Storage (ES) function, usually achieved via rechargeable batteries, can be combined with its pointing system (i.e. the Attitude Control Subsystem (ACS)), forming an Energy Storage and Attitude Control System (ESACS) [5]. Such an ESACS typically consists of flywheel-based, three-axis stabilising, momentum exchange actuators such as Reaction Wheels (RWs), Momentum Wheels (MWs), Control Moment Gyroscopes (CMGs), or Variable-Speed CMGs

*Graduate Student, Surrey Space Centre, School of Electronics and Physical Sciences, University of Surrey. Email: d.richie@surrey.ac.uk. Senior member AIAA.

†Lecturer, Surrey Space Centre, School of Electronics and Physical Sciences, University of Surrey. Email: v.lappas@surrey.ac.uk. Member AIAA.

‡Reader, Surrey Space Centre, School of Electronics and Physical Sciences, University of Surrey. Email: p.palmer@surrey.ac.uk. Member AIAA.

§The views expressed in this article are those of the authors and do not reflect the official policy or position of the United States Air Force, Department of Defense, or the U.S. Government

(VSCMGs) doubling as energy storage devices. RWs provide zero-biased momentum through low spin rates thus are unrealistic for energy storage. In contrast, MWs have a momentum bias through non-zero nominal spin rate and thus the ability to store and drain flywheel energy, while CMGs operate at fixed flywheel speeds without freedom to store and drain energy. However, the CMG torque amplification property in which a small amount of CMG gimbal motor input torque results in a relatively large slewing torque, gives it a distinct advantage over a MW-based system [6]. Fortuitously, VSCMGs combine these CMG and MW advantages while eliminating well-known CMG gimbal-lock singularities and therefore are the most logical ESACS alternative.

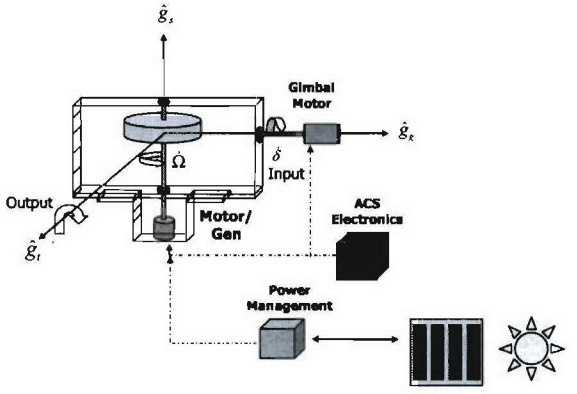

Fig. 1 VSCMG Principles of Operation

State-of-the-Art Review

Although the flywheel energy storage concept predates the potter's wheel, Roes was apparently the first to propose its use in satellites in 1961 [7]. However, it was not until the early 1970s, during the international energy crisis, when coupling Roes' approach with the attitude control function emerged [8–14], spawning several proposals for an ESACS, primarily for employment on NASA's International Space Station (ISS). As this technology progressed, designers encountered flywheel rotor material and mechanical bearing/levitation issues [15, 16]. Likewise, many of these early concepts relied on counter-rotating MW implementations while a handful mentioned CMGs as plausible alternatives. Then, the development of hybrid cars propelled flywheel energy storage technologies such as composite rotors and magnetic bearings to burgeoning maturity [17]. This sparked renewed interest in ESACS in parallel with ISS advancing development. Key related results included Chris Hall's gyrostat investigation [18] and Shen, Tsiotras, and Hall's simultaneous control design for an ESACS subcategory, an Integrated Power and Attitude Control System (IPACS), using four redundant, non counter-rotating, momentum wheels [19]. In parallel to these efforts, Hall gave an excellent pre-2000 literature review for this problem in [20]. One should refer to that document for a further list of significant contributions.

Nevertheless, building on Shen, Tsiotras, and Hall's work, Richie, Tsiotras, and Fausz [5] showed simultaneous momentum wheel and gimbal control were possible by employing the new momentum exchange device theoretical generalization known as the VSCMG, conceptualized by the combined efforts of Ford and Hall [21, 22] and Schaub, Junkins, and Vadali [23]. The VSCMG development, of course, was predicated on the detailed CMG theory offered by Jacot and Liska [24], Marguilles and Aubrun [25], Oh and Vadali [26], Wie [27], and several others [28–30]. Following Richie, Tsiotras, and Fausz' work, Yoon and Tsiotras identified a wheel speed equalization technique for reducing the risk that one VSCMG reaches saturation, effectively increasing a VSCMG-suite's utility [?, ?]. Other related work involves Roithmayr's VSCMG-gyrostat generalization to gimballed, counter-rotating wheels including satellite to actuator damping torque [31] with direct application to systems with a mixture of counter-rotating MWs and standard CMGs.

Heretofore, ESACS performance was limited due to bearing friction and structural fatigue, hurdles virtually eliminated by composite material and magnetic bearing advances. Without these barriers, two major contemporary ESACS programs targeted for medium to large satellites stand to gain from this technology, NASA's counter-rotating wheels [32–34] and the US Air Force Research Laboratory's VSCMG-like ESCMG work [35], both focused on laboratory validation prior to flight. In contrast, small satellite implementation of ESACS VSCMGs has not been done. Only recently has the dogma of CMG-use for large satellites been exploded with Lappas' small satellite work [6]. Likewise, Varatharajoo demonstrated small satellite counter-rotating MW ESACS use [36]. Neither of these efforts address using VSCMGs in an ESACS role. Thus, one needs to extend Lappas' and Varatharajoo's work by defining an algorithm for adequately sizing such VSCMGs for an ESACS. Identifying this algorithm is the sole aim of this paper.

In meeting this objective, the paper is organized as follows: section 2.0 describes the benefits for a VSCMG-based ESACS; section 3.0 presents the key technology trades required in selecting such a system; section 4.0 gives ESACS fundamentals including describing the key design margin definitions; section 5.0 addresses the applicable decision variables, constraints, and objective function that define the optimal ESACS VSCMG sizing nonlinear programming problem; section 6.0 illustrates two general design objective categories, design for equivalent performance and design for equivalent mass as compared to a contemporary baseline; section 7.0 presents example results from applying this algorithm to a space RADAR mission; section 8.0 identifies future work building on these results; and section 9.0 summarizes this investigation's key findings.

2.0 ESACS Benefits

An ESACS brings several advantages to a small satellite, including significant mass savings, longer lifetime, favourable power density, moderate energy density, and increased satellite agility as compared to a contemporary 4-MW ACS plus Nickel Cadmium (NiCd) battery ES. Mass savings follows from function consolidation. Consider a 400 kg satellite which includes a 40 kg MW-based ACS plus NiCd ES. If one were to replace the ACS plus ES with a VSCMG-based ESACS at a mass of 20 kg, the gain would be a 50% mass savings at the subsystem level and a 5% mass savings at the satellite level, a profound cost benefit.

Second, as shown by Lappas in [6], a small satellite with its CMG torque amplification advantages yields a tenfold increase (1.0 to 10.0 °/s as compared to 0.1 to 1.0 °/s for MWs) in slew rate for a system of equivalent size/mass. Plus, the VSCMG-based ESACS' variable-speed property permits better singularity avoidance characteristics [37].

Third, satellite lifetime, shown in Figure 2 for contemporary technologies plus flywheel batteries, increases for a given VSCMG battery depth-of-discharge (DOD), the percent of total capacity removed from the battery, as compared to its conventional counterpart. Clearly, lifetime drops off linearly with increased secondary battery DOD. This makes sense – the greater average depth one draws down a battery during discharge cycles, the quicker the battery will wear out. However, even if these secondary battery limits did not hold, most contemporary satellites would not last more than 83000 cycles due to solar panel lifetime limits (assumed to be 15 years in LEO). For this reason, the Li-ion data is cut off at 83000 cycles. Similarly, one can assume satellites using flywheel batteries are limited by this solar panel degradation constraint. Contrary to secondary batteries, though, VSCMG batteries can sustain this lifetime for various DOD levels. The result is longer VSCMG battery lifetime at high DOD levels. For this paper, a conservative VSCMG battery DOD limit of 80% is assumed (allowing 20% for attitude control safety margin). Comparing this to the typical LEO satellite secondary battery value of 15-20% DOD, one can

see the lifetime advantage of a VSCMG-based ESACS. The last

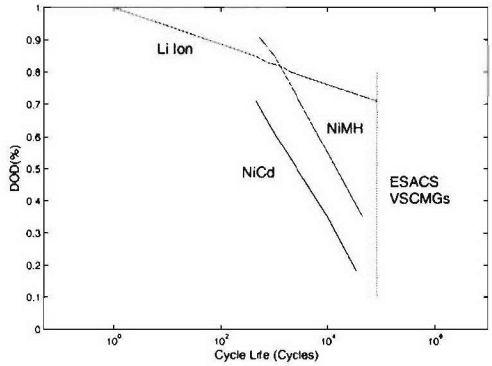

Fig. 2 Depth-of-Discharge Versus Lifetime

advantage follows from comparing popular secondary battery energy storage approaches (Lithium-Ion (Li-Ion), Nickel Cadmium (NiCd), and Nickel Metal Hydride (NiMH)) to flywheels. Although a satellite's storage capacity is important, the producible peak power during discharge is paramount to high-power operations in eclipse. The designer needs to know a proposed ES's ability to store and drain energy as related to the most crucial satellite commodity – mass. Figure 3's Ragone Plot, constructed from contemporary battery data including that used in SSTL small satellites, captures this idea in each technology's energy versus power density plots. The dashed lines represent the theoretical boundaries for these technologies. Also, several patched data points represent actual data adjusted for VSCMG comparison as typical Energy and Power densities use the per-cell mass, not the entire EPS mass. Moreover, in the case of ESACS, one needs the combined ACS and ES system mass, dividing these densities by this value. The true comparison occurs in evaluating the flywheel-based VSCMG data points in the upper right quadrant of Figure 3 versus the data points in the lower left. Clearly, VSCMG ES has power and energy density advantages. Even if the plotted Lithium Ion battery performance was based on the entire ACS plus ES mass, that result still falls short of the VSCMG battery's true strength–power density. This means that a high peak power system like a satellite RADAR is better powered through flywheel batteries than Lithium Ion.

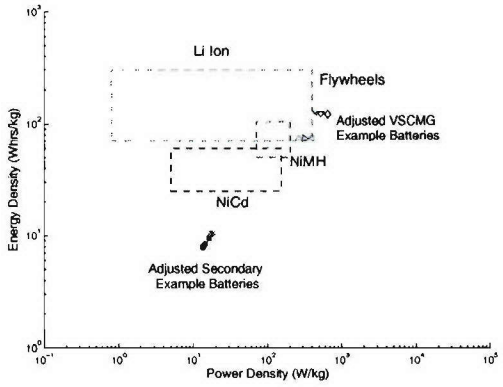

Fig. 3 Ragone Plot

3.0 Design Alternatives

Despite past barriers, several flywheel energy storage schemes have been proposed which incorporate its constituent technologies (e.g. composite rotors, high-spin compatible bearings, and advanced motor/generator electronics). The set of realistic VSCMG ESACS technologies is captured in the Figure 4 Design Trade Tree. The items shown in Figure 4 are the realistic, contemporary options from past, present, and short-term proposals in the literature. This trade tree defines the essential hardware trade space and bounds VSCMG design approaches. In fact, the three investigated design alternatives encompass the most promising combinations from this tree. Before identifying these alternatives, one must understand a key trade space feature. As Henrikson, Lyman, and Studer state in [38], "the development of magnetically suspended momentum wheels is just beginning. There is no tendency as yet for designs to settle on one or two 'best' configurations, but rather there are nearly as many configurations and design opinions as there are workers in the field." This applies not just to the magnetic suspension, but also to the layout of the flywheel, the rotor construction, the motor/generator design, and the implemented power and attitude control electronics.

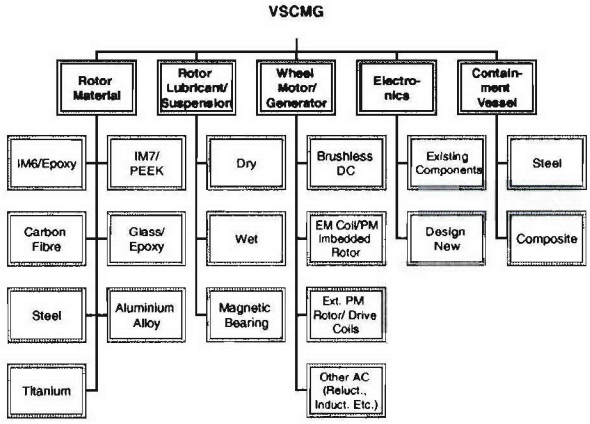

Fig. 4 Full VSCMG Design Trade Tree

Nevertheless, several observations lead one to prune the trade tree most effectively and identify the best technologies. First, although mechanical (wet and dry) lubricants work well for most terrestrial applications, these devices are limited in space utility. A better alternative lies in magnetic bearing suspension, from the complex 5 degree of freedom (5-DOF) approach, to the simpler but less forgiving 1- and 2-DOF versions. As Varatharajoo addressed, the 2-DOF method is best for small satellites [36], thus the magnetic-bearing trades addressed here imply the 2-DOF option. Also, the electronics yield two options: use existing electronics or design new ones. In keeping with this effort's aim for low-cost, SSC/SSTL synergy, reusing existing electronics is best. Likewise, two basic containment vessel classes (of hundreds) dominate – steel and composites. For reduced wheel speed applications, Lappas' adaptation of common SSTL electronics trays as containment vessels makes sense. However, larger applications require crafting an individual VSCMs container, presumably made of Kevlar. Finally, identifying the power bus design is important. There are two primary conventional types as defined in [39], Peak Power Tracker (PPT) or Direct Energy Transfer (DET) and a hybrid of the two such as done by Clark approach [40]. In maintaining SSC/SSTL synergy, since the PPT approach is more prevalent amongst SSTL satellites, this method will be employed here.

As for designs, Alternative #1 uses a bolstered SSC CMG design with a high-speed wheel rotor and motor/generator. Alternative #2 uses an open motor concept based on individually-wound, external magnetic coils which propel a ring of magnetic material affixed to the rotor. Likewise, a second set of coils are used as power generator coils to drain energy from the rotating wheel. This wheel is magnetically levitated via a hub-based magnetic bearing similar to that used by Varatharajoo [36]. Finally, Alternative #3 uses rotor-imbedded motor and generator coils with a hub-based magnetic bearing like that of [36].

4.0 ESACS Fundamentals

To achieve success, the ESACS engineer needs system design margins (i.e. the differences between the actual design and its associated requirement) that are at or above 0. Identifying the requirements for the 4 key parameters, torque, peak power, storage capacity, and mass, N_r, P_r, C_r, and M_r, respectively, and actual equivalents, N_a, P_a, C_a, and M_a, one can define the relevant design margins, N_m, P_m, C_m, and M_m

$$N_m = N_a - N_r \quad (1)$$
$$P_m = P_a - P_r = N_{vc}P_{a_1} - P_r \quad (2)$$
$$C_m = C_a - C_r = N_{vc}C_{a_1} - C_r \quad (3)$$
$$M_m = M_r - M_a = M_r - N_{vc}M_{a_{1_i}} \quad (4)$$

where

$$N_a = \xi I_{w_s}\Omega_{min}\dot{\delta}(2+2\cos\beta) \quad (5)$$
$$N_r = \frac{4I_{T_{max}}\theta_f}{(t_f^2 - t_{off}^2)} \quad (6)$$
$$P_{a_1} = I_{w_s}(\Omega_{max} - \Omega_{min})\dot{\Omega} \quad (7)$$
$$C_r = \frac{d_{ty}T_eP_r}{dodx_{msn}} \quad (8)$$
$$C_{a_1} = k_s\sigma_\theta\pi l_{rot}\left(r_o^2 - r_i^2\right)\left(1 - \left(\frac{\Omega_{min}}{\Omega_{max}}\right)^2\right)/3600 \quad (9)$$

$$M_{a_{1_1}} = m_{rot}(l_{rot}) + m_{oth}(l_{rot}) + m_{kii_{scaled}} + m_{dc_{scaled}} \quad (10)$$
$$M_{a_{1_2}} = m_{rot}(l_{rot}) + m_{oth}(l_{rot}) + m_b(l_{rot}) + 2m_{m_2}(l_{rot}) \quad (11)$$
$$M_{a_{1_3}} = m_{rot}(l_{rot}) + m_{oth}(l_{rot}) + m_b(l_{rot})m_{m_3}(l_{rot}, \Omega_{max}) \quad (12)$$

and $I_{w_s} = 0.5\pi\rho_{rot}l_{rot}\left(r_o^4 - r_i^4\right)$. P_r and M_r are given by mission requirements. Furthermore, Equations 1, 2, and 3 ensure the actual values are greater than or equal to the required values when the design margins are non-negative. A feasible (i.e. usable) design is thus defined as one in which the design margins are non-negative. Only feasible designs are considered.

Next, 5 variables drive the design margins and are thus interrelated: Ω_{max}, Ω_{min}, l_{rot}, $\dot{\Omega}$, and σ_θ/ρ_{rot}. Selecting these parameters, known as decision variables, via an optimal sizing algorithm is addressed next. Furthermore, these parameters are constrained in that Ω_{max}, Ω_{min}, l_{rot}, $\dot{\Omega}$, σ_θ/ρ_{rot} plus N_m, P_m, C_m, and M_m must be non-negative for design feasibility. Added to this, Ω_{max} is structurally limited by the flywheel rotor strength, Ω_{min} is limited in ensuring enough torque and power is produced by the flywheel, and the disparity between the maximum and minimum allowable wheel speeds is limited to ensure proper energy is stored. Thus, these constraints drive these five feasible ESACS design variables.

5.0 Optimal Actuator Sizing

Designing effective ESACS VSCMGs centers on selecting the best decision variable combination (i.e. that optimizes a suitable performance index) to meet mission requirements subject to the aforementioned constraints. Since an underlying aim in this task is to produce a system that outperforms the baseline MW ACS plus NiCd ES, a performance index, J, was crafted to capture the relationship of the ESACS design to the baseline. It is defined as the ratio of the four VSCMG design margins to baseline counterparts

$$J = \frac{C_mP_mN_mM_{m_i}}{C_{m_b}P_{m_b}N_{m_b}M_{m_b}} = \frac{N_{vc}{}^3C_{m_1}P_{m_1}N_mM_{m_{i1}}}{C_{m_b}P_{m_b}N_{m_b}M_{m_b}} \quad (13)$$

where the index $i = 1$, 2, or 3 relates to the candidate alternative in consideration (i.e. #1, #2, or #3) and its differently calculated mass. The capacity and power margins are calculated based on one VSCMG as is the mass margin, but the torque margin (as are the baseline margins) is calculated for the entire VSCMG suite. This has been included in finding J. Furthermore, for the best ESACS to baseline ratio one needs to maximize $J = value$, or equivalently, minimize $J = -value$. Incorporating the constraints, one can cast the problem as a standard Nonlinear Programming Problem (NLP):

Minimize

$$J = -\frac{N_{vc}{}^3C_{m_1}P_{m_1}N_mM_{m_{i_1}}}{C_{m_b}P_{m_b}N_{m_b}M_{m_b}}, i = 1,2,3 \quad (14)$$

Subject to

$$C_{m_1}, P_{m_1}, N_m, M_{m_{i_1}} \geq 0 \; i = 1,2,3 \quad (15)$$
$$\Omega_{max}, \Omega_{min}, l_{rot}, \dot{\Omega} \geq 0 \quad (16)$$
$$\left(\Omega_{max}^2 - \Omega_{min}^2\right)l_{rot} \geq \frac{4T_eP_r}{N_{vc}\pi\rho_{rot}(r_o{}^4 - r_i{}^4)} \quad (17)$$
$$\Omega_{max} \leq \Omega_{struct} \quad (18)$$
$$l_{rot} \leq l_{real} \quad (19)$$
$$\dot{\Omega} \leq \dot{\Omega}_{real} \quad (20)$$
$$J \leq -1.0 \quad (21)$$

where Ω_{struct} follows from applying the radial force equilibrium equations defined by Danfelt et. al. and addressed in Varatharajoo [36,41] for a typical, anisotropic (orthotropic), single-layer rotor. Captured directly from [36,41,42], the governing stress equations for a constant speed flywheel are:

$$\sigma_r = \alpha_1\frac{E_r(\lambda + \nu_{\theta r})}{(1 - \nu_{\theta r}\nu_{r\theta})}r^{\lambda-1} + \alpha_2\frac{E_r(\nu_{\theta r} - \lambda)}{(1 - \nu_{\theta r}\nu_{r\theta})}r^{-\lambda-1} - \frac{(3 + \nu_{\theta r})\rho\Omega^2}{9E_r - E_\theta}r^2 \quad (22)$$

$$\sigma_\theta = \alpha_1\frac{E_\theta(1 + \lambda\nu_{r\theta})}{(1 - \nu_{\theta r}\nu_{r\theta})}r^{\lambda-1} + \alpha_2\frac{E_\theta(1 - \lambda\nu_{r\theta})}{(1 - \nu_{\theta r}\nu_{r\theta})}r^{-\lambda-1} - \frac{(1 + 3\nu_{r\theta})E_\theta\rho\Omega^2}{9E_r - E_\theta}r^2 \quad (23)$$

The integration constants, α_1, α_2, are found by applying radial stress boundary conditions (i.e. $\sigma_r = 0$ at $r = r_o$ and $\sigma_r = -t_{sp}\rho_{sp}\Omega^2r_i^2$ at $r = r_i$). Substituting these 2 values in equations 22 and 23, one can calculate the stress distribution in the wheel for a given wheel speed, or conversely, use the maximum allowable rotor stress to define the maximum allowable wheel speed. The latter of these techniques yields Ω_{struct}. The stress distribution can be viewed graphically in figures 5 and 6 which directly follow from [41] and [36]. In these plots, the allowable stress (tensile and compressive) values are superimposed upon the stress distribution plots for determining the maximum allowable structural wheel speed.

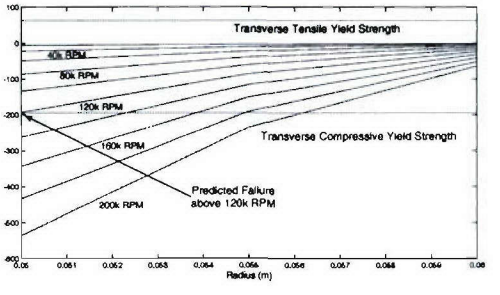

Fig. 5 T1000G Carbon Fiber Radial Stress Distribution

To solve the optimal problem proposed in Equations 14 and 15, one must understand a few basic principles. As explained in [43], an optimal parametric design is achieved by crafting the Hamiltonian (the Lagrangian plus the linear combination of nonlinear

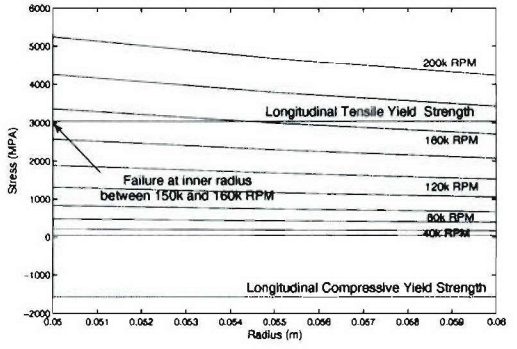

Fig. 6 T1000G Carbon Fiber Tangential Stress Distribution

constraints), then setting its first derivative equal to 0 to find inflection points, and completed using the second Hamiltonian derivative to determine if the inflection points are local maxima, local minima, or saddle points. Here, the Hamiltonian is formed by adding to the performance index equation the sum of each constraint multiplied by a multiplication constant (aptly termed a "Lagrange multiplier"). If the performance index or the constraints are nonlinear, as in the VSCMG-based ESACS optimal actuator sizing case, the problem is known as an NLP.

Figure 7 illustrates the basic optimal actuator sizing process as incorporated in the authors' Microsoft Excel Solver-based VSCMG ESACS sizing tool. The process includes mission and

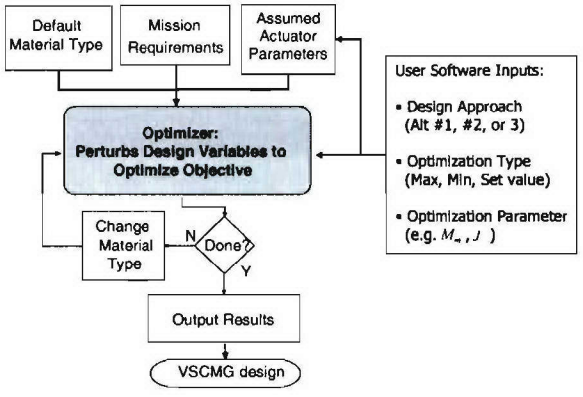

Fig. 7 Basic Optimal Sizing Process

actuator parameter definition; user inputs (alternative number, optimization type, and optimization parameter selection (J, M_m)); optimizer operation; and design outputs for different combinations of σ_θ/ρ_{rot}. On a basic level, the optimizer performs the standard parametric design optimization mentioned above, but uses an iterative reduced order gradient algorithm designed to reduce the number of computations required for multiple-decision variable problems with hundreds of decision variables as well as robust error checking code to trap user input errors. Here, the primary optimizer function generates a single point design for alternative (#1, #2, or #3), type (minimize, maximize, or set a certain value for a chosen parameter), and optimization parameter (J, M_m). Then, another function generates multiple point designs through several individual optimizations (batch mode) for different key parameters, specifically $\dot{\Omega}$ and the material type. These results can then be reviewed, scored, and evaluated in selecting a design.

6.0 Analysis Objectives

Applying actuator optimization technique depends on the desired objective. In the continuous effort to reduce mass, one obvious approach is to optimize the ESACS to baseline mass savings at equivalent performance. An alternative (but arguably equally important) goal is to maximize the ESACS to baseline performance at equivalent mass. This method is akin to answering a small satellite customer's question, "How much agility/peak power/capacity improvement over the baseline system can ESACS provide my experimental at an equal mass?" This is especially significant when such a customer equates mass to mission cost (price).

Either approach involves further constraining the basic optimal sizing problem (i.e. adding more constraint equations to the presented NLP). In the case of equivalent performance, the ratio of $P_m C_m N_m$ must equal $P_{m_b} C_{m_b} N_{m_b}$ such that the performance index is based on M_m optimization. However, from a scientific method perspective, this approach has one obvious flaw–individual margins P_m, C_m, and N_m can have several values as long as the product equates to $P_{m_b} C_{m_b} N_{m_b}$. This can yield several different results with non-readily apparent benefits. Thus, a more accurate implementation is to individually equate these margins such that $P_m = P_{m_b}$, $C_m = C_{m_b}$, and $N_m = N_{m_b}$, permitting a controlled implementation in which only M_m changes through decision variable selection.

Interestingly, these constraints force an analytic solution to the problem, which can then be used to validate the results. The basic idea is to substitute the baseline margin values into equations 1, 2, and 3. Setting $C_{m_1} = C_{m_b}/N_{vc}$, $P_{m_1} = P_{m_b}/N_{vc}$, and $N_m = N_{m_b}$, and defining constant values c_1, c_2, and c_3, one finds

$$c_1 = \left(\frac{{\Omega_{max}}^2 - {\Omega_{min}}^2}{{\Omega_{max}}^2}\right) l_{rot} = \frac{3600\left(C_{m_b} + \frac{d_{ty} T_e P_r}{dod x_{msn}}\right)}{N_{vc}\sigma_\theta k_s \pi\left({r_o}^2 - {r_i}^2\right)} \quad (24)$$

$$c_2 = l_{rot}\left(\Omega_{max} - \Omega_{min}\right)\dot{\Omega} = \frac{2\left(P_{m_b} + P_r\right)}{\rho_{rot} N_{vc} \pi\left({r_o}^4 - {r_i}^4\right)} \quad (25)$$

$$c_3 = \Omega_{min} l_{rot} = \frac{2\left(N_{m_b} + \frac{4 I_{sc}\theta_f}{t_f^2 - t_{off}^2}\right)}{\pi\rho_{rot}\left({r_o}^4 - {r_i}^4\right)\xi\dot{\delta}(2 + 2\cos\beta)} \quad (26)$$

Also, notice that each of these equations can be expressed as a product of a material property ($(1/\sigma_\theta)$ or $(1/\rho_{rot})$) and a fixed constant. Combining the c_1, c_2, and c_3 equations and re-arranging yields:

$$\Omega_{min} = \left(\frac{{c_2}^2 c_3 + 2 c_2 {c_3}^2 \dot{\Omega}}{c_1 {c_2}^2 + 2 c_1 c_2 c_3 \dot{\Omega} + c_1 {c_3}^2 \dot{\Omega}^2}\right) \quad (27)$$

$$\Omega_{max} = \left(\frac{{c_2}^3 c_3 + 3 {c_2}^2 {c_3}^2 \dot{\Omega} + 2 c_2 {c_3}^3 \dot{\Omega}^2}{c_1 {c_2}^2 c_3 \dot{\Omega} + 2 c_1 c_2 {c_3}^2 \dot{\Omega}^2 + c_1 {c_3}^3 \dot{\Omega}^3}\right) \quad (28)$$

$$l_{rot} = \left(\frac{c_1 {c_2}^2 + 2 c_1 c_2 c_3 \dot{\Omega} + c_1 {c_3}^2 \dot{\Omega}^2}{{c_2}^2 + 2 c_2 c_3 \dot{\Omega}}\right) \quad (29)$$

This final equation set illustrates the direct dependency of Ω_{min}, Ω_{max}, and l_{rot} on $\dot{\Omega}$ when ESACS to baseline performance is equal.

Likewise, for the equivalent mass problem, one needs to further constrain the basic NLP through equating the mass margins, i.e. $M_m = M_{m_b}$. However, in this case, there is more design freedom to choose results and an analytic solution isn't as easy to find, especially since 2 of the mass equations rely on l_{rot} only whereas one relies on l_{rot} and Ω_{max}. If, for example, a constraint is added, such as $N_m = N_{m_b}$, which is realistic in the case of the satellite customer that only desires equivalent torque (i.e. agility) at equivalent mass, but desires increased energy storage and/or peak power demand to operate an experiment, a similar set of analytic equations can be found when the mass only depends upon rotor length, l_{rot}.

Thus, there are 2 primary approaches in comparing the designed ESACS with the baseline system, equivalent performance and equivalent mass, both of which yield utility to satellite mission developers. The former of these approaches, equivalent performance, is illustrated in the ensuing optimal sizing example.

7.0 Optimal Sizing Example

Mission Description, Requirements, and Actuator Assumptions

Generally, a Synthetic Aperture RADAR (SAR) permits high-resolution images be crafted from several consecutive target returns using a small antenna vice the large, conventional high-resolution microwave RADAR antennas [44]. Stripmapping SAR is "the oldest and most widely known form of SAR ... in which the antenna remains fixed with respect to the RADAR platform so that the antenna beam sweeps out a strip on the ground" [44]. This is quite similar to the conventional push-broom technique used in satellite imaging cameras. Clearly, space-borne RADAR, being employed in the ultimate high ground, have an immense coverage advantage over airborne, ship-borne, and ground-based RADAR with a disadvantage in resolution. Although stripmapping SAR yields efficient resolution for antenna size, Spotlight mode SAR, in which the "the antenna is steered to continuously illuminate a single [target]," thereby illuminating it from several different angles, is an even more accurate technique when collecting high-resolution data from a small object [44].

Obviously, the farther away the satellite is from a target the more precise the SAR's attitude control must be to maintain the desired resolution. Whereas stripmapping SAR requires a fixed platform for the camera during imaging, Spotlight SAR requires the camera be constantly slewed. Similar to the UK-DMC imaging mission, there are 2 primary design strategies to meet the individual mini-Spotlight SAR satellite's pointing needs: rapidly slew the entire satellite with a rigidly attached dish, or, maintain a fixed orientation (e.g. continual nadir/Earth pointing) whilst scanning the dish. Although each approach has its challenges, the former makes sense due to recent advancements in spacecraft agility. This permits using a standard, agile platform across SAR systems without custom designing a slew-able RADAR dish for each mission. Plus, due to the complex data and its required processing, storage, and retrieval, such a system needs large instantaneous peak power for collecting and transmitting data to the ground. From this, the SAR satellite requires high instantaneous peak power to operate and is often used during eclipse, levying a huge energy storage burden.

Table 1 Space RADAR Requirements

Parameter	Value
Orbit Altitude, h, km	450
Depth-of-Discharge, dod, %	80
Transmission Efficiency, x_{msn}, %	90
Peak Power Demand, P_r, W	1100
Eclipse Duty Cycle, d_{ty}, %	25
Power Bus Voltage, V_{bus}, V	28
Max Single-axis inertia, $I_{T_{max}}$, kgm^2	120
Slew maneuver angle, θ_f, deg	140
Slew maneuver time, t_f, s	70
Slew maneuver dead-band, t_{off}, s	12
Satellite Total Mass, M_{sc}, kg	400
Allowable Satellite Mass, M_{ta}, kg	450
Allowable ACS plus ES Mass, M_r, kg	45

As implied earlier, the key ESACS requirements are the instantaneous Peak Power demand, P_r, and the required maneuvering torque from the actuators, N_r, in this case assumed to be for a bang-off-bang maneuver as previously parameterized. Table 1 gives the assumed parameters for this maneuver (i.e. a 140° maneuver in 70 s with a 12 s dead-band and 1100 W instantaneous peak power with a maximum principle-axis of inertia of 120 kgm^2). These requirements follow for the near-term small satellite Space RADAR mission and represent a tenfold increase in slew maneuvering and energy storage over a nominal SSTL-built small satellite.

Assumptions

Before examining the results from this example, it's important to identify a few key assumptions. First, rotor containment in the event of catastrophic wheel failure is VERY important to personnel and systems safety in testing the proposed hardware. As previously stated, the simpler containment approach (i.e. designed for a much smaller satellite CMG system) is not sustainable in this configuration. Thus, a new containment solution will probably entail the use of a Carbon Kevlar flywheel envelopment.

Second, there are several different schemes for wheel spin initialization once the satellite is deployed. This study has not ventured to explore all of these, but awareness of this issue is paramount to future on-orbit success. Plausible methods include EPS battery-like trickle charging; solar panel to super capacitor to VSCMG ESACS charging; or employment of a small primary battery to handle the power load until the VSCMGs are adequately charged to commence on-orbit operation.

Third, this technology only applies for missions with simultaneous high precision pointing and high peak power requirements. If either requirement is eliminated, this approach loses its utility.

Fourth, the presented arguments focus on this technology's role in fulfilling the entire energy storage mission for a satellite, however, an equally plausible (if not better) alternative is to employ VSCMG ESACS on precision pointing missions wherein a system (e.g. a high-power, high-agility payload) only needs the high-power properties of the ESACS during some operations, but does not need them all the time. Thus, the EPS can supplement the VSCMG flywheel batteries with conventional secondary ones. This synergy could prove quite beneficial.

Mass Savings and Performance Index Optimization Results

One can now couple the SAR mission requirements with actuator assumptions (which vary by design alternative), and then evaluate different ESACS VSCMG point designs. This is done for the equivalent performance case. The ensuing results are visually conveyed 2 ways: i) wheel acceleration, $\dot{\Omega}$, versus mass savings plots by material type and ii) optimal decision variable plots (i.e. of the I_{rot} versus Ω envelope, Ω_{min} to Ω_{max}, for several values of $\dot{\Omega}$ and grouped by material type and alternative). After assessing this data, the maximum mass savings results are combined with the maximum performance results and tabbed via a scoring method. These scores are then rank ordered and analysed in order to select the most appropriate designs.

Figures 8 and 9 show the mass savings and performance index values, respectively, for selected materials as a function of wheel acceleration, $\dot{\Omega}$, evaluated for the equivalent performance case. As one can see, composites consistently outperform metal materials via mass advantages with equitable strength. The top performing rotor material is T1000G Carbon fiber, perhaps the strongest of the composites (and all materials considered in this study) for its mass, using Alternative #3 – the magnetic bearing-based design similar to the one defined in [36]. Also fairing well were the other composites, mostly enjoying 50 + % advantage over the baseline, which was quite close to the Metals results. The results from Figure 8 apply when $C_{m_1} = C_{m_b}/N_{vc}$, $P_{m_1} = P_{m_b}/N_{vc}$, and $N_m = N_{m_b}$. For the most part, the trends are linear, with a downward slope. This slope follows from motor/generator and/or magnetic bearing mass demanded of systems that produce higher torque (i.e. acceleration). The increase in mass causes the system mass savings to drop with $\dot{\Omega}$. In a few instances (namely Glass/Epoxy Alternative #2), the rotor length limit is reached before the highest wheel acceleration is reached, thus cutting out any increase in length, associated decrease in mass, and ending any decrease in performance versus the baseline. Simply put, this effect is the sizing saturation imposed by the rotor length constraint.

In examining the performance index plot, figure 9, one can get a more direct feel for how a design compares to the baseline. The

idea is that J values < -1.0 yield performance better than the baseline. Again, Carbon fiber T1000G Alternative #3 leads the pack with the lowest J value, followed closely by composites IM6/Epoxy and IM7/PEEK. Interestingly, these materials perform up to 3 times better than the baseline, with the lion's share besting the baseline at a two-to-one ratio.

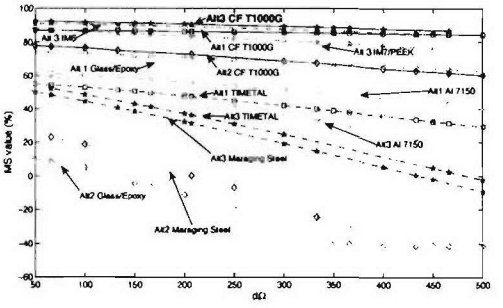

Fig. 8 Material Mass Savings at Equal Performance

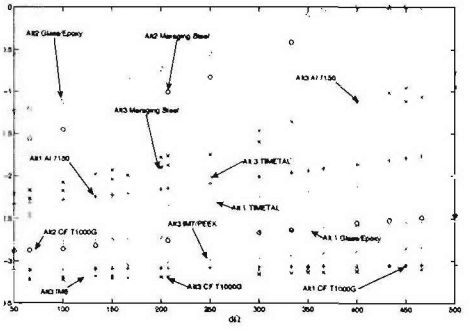

Fig. 9 Material Performance Index at Equal Performance

The decision variables themselves can also be combined into a single plot like Figure 10, wherein point designs for the T1000G Carbon fiber-based Alternative #3 are displayed. The horizontal axis is rotor length and the vertical axis wheel speed. Each vertical line corresponds to a different maximum wheel acceleration ($\dot{\Omega}$) setting. In other words, a vertical line for each value of $\dot{\Omega}$ is plotted for rotor length with its vertical axis magnitude running from Ω_{min} to Ω_{max}.

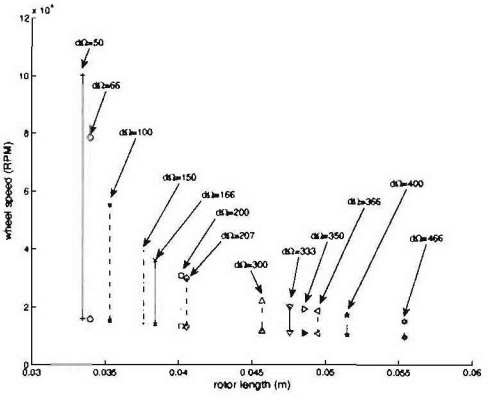

Fig. 10 Decision Variables Example Plot: Alternative #3 Carbon fiber

This plot helps the designer evaluate point designs through examining decision variables. For instance, one can see that Alternative #3 with a Carbon fiber rotor and $\dot{\Omega} = 150\,\mathrm{rad/s^2}$ uses a rotor length of 0.038 m and has wheel speed limits of 15000 RPM to 40000 RPM. Qualitatively, one can see that as $\dot{\Omega}$ increases, rotor length increases, minimum wheel speed decreases (but only slightly), and maximum wheel speed decreases quite drastically. These plots help the designer understand design limits both qualitatively and quantitatively. Plus, the shape of the decision variable plot changes when using a different optimization type (e.g. minimize J rather than maximize Mass Savings). Such a plot is *an* indicator, but not *the* indicator of the best design for a set of requirements. However, it can be coupled with plots like those of the Mass Savings and Performance Index results presented earlier to determine advantageous designs. For example, knowing that a design gives 40-50 % Mass Savings doesn't help the designer know the dimensionality of that VSCMG design or its wheel speed range. Having a plot like Figure 10 solves that problem. Logically, the best designs follow from small rotor length and a good minimum-maximum wheel speed spread (i.e. where there is a sufficient wheel speed operating range) – the more maneuvering room within wheel speed limits, the more the overspeed/underspeed error margin for the wheels and the more possible ESACS solutions with smoother dynamics are possible. However, high values for rotor length and maximum wheel speed are more difficult to implement in the hardware. Thus, one can use the mass savings and decision variable plots to get a feel for how each material type and alternative affect the design.

Scoring the Design Alternatives

The final design process step is to score the alternatives. The chosen scoring method combines optimizations for maximising Mass Savings (with baseline-equivalent performance) and minimising the performance index (with 0% Mass Savings). For the SAR mission, the latter of these 2 necessarily makes for a very large, unrealistic rotor length to increase design margins. This yields a large, negative-valued performance index, J). One way to limit this unrealistic result is to constrain the maximum rotor length. However, this prevents the Mass Savings from being 0%. Nevertheless, the results here were generated by keeping the rotor length within a fairly realistic range using different constrained values for the MS maximization problem than for the performance index minimization problem.

Point Designs

In scoring the results for the equivalent performance case, it was found that the best scoring flywheel rotor material is Carbon fiber and the best design method is Alternative #3. Logically, the top scored design occurred at the highest (but not yet achievable) angular acceleration used, $\dot{\Omega} = 500\,\mathrm{rad/s^2}$. As reflected in Figure 10, if one reduces the wheel acceleration requirement, the wheel speed range increases quite drastically (i.e. moving right to left on the plot). This is important since one method of realising such a system (with an incremental development approach) involves building each of the point designs from left to right (i.e. start at an achievable wheel acceleration and increase capability by changing the motor and wheel speed range). However, a better approach is to choose a realistic future design (in the 5-10 year time frame) in terms of required angular acceleration that operates in a realistic wheel speed range (e.g. 20000 RPM to 55000 RPM), then build the VSCMG to sustain these limits, starting at a realistic wheel acceleration while gradually increasing to the long-term, wheel acceleration point design. This refined implementation strategy requires changing the motor as torque capability increases assuming wheel speed remains constant. This follows typical DC motor capability theory – a motor's capability is assessed by its torque-speed curve where the motor speed is traded for its torque. Also, every motor's torque-speed curve has capability limits (i.e. the stall torque and the no-load speed). Therefore, as motor technology improves, motor torque-speed limits increase. Thus, this design approach calls for setting the wheel no-load speed limit and applying stall torque improvements as they occur (i.e. which are proportional to wheel

acceleration improvements).

Put another way, DC motor output power is the torque-speed product. Thus, conventional DC motors are rated by shaft power. COTS versions for small applications typically operate peak between the 10-200 W range, with a few designs in the 100-350 W range. Custom-built motors are the only contemporary choices that exceed the 400 W realm. This is important as the desired long-term design calls for 576 W output power per each of the VSCMG wheel in order to meet the mission requirements. Small motors operating at such high power also incur large thermal losses, further restricting effective employment for VSCMG ESACS.

In summary, the Carbon fiber rotor design has been identified as the best long-term VSCMG design for a small satellite ESACS using Alternative #3. Actualising it requires 2 major advancements: a COTS motor/generator system that can accelerate the wheel at high acceleration and a COTS miniature magnetic bearing to suspend its flywheel. Lack of miniature COTS magnetic bearings drive the selection of two different designs–one that uses the magnetic bearing (Alternative #3) and one that does not (Alternative #1).

Defining the Baseline MW/NiCd System

The designs from the previous section can be compared to the baseline in order to determine VSCMG-based ESACS effectiveness. However, before comparing these designs, it helps to review the baseline design and its margins. First, since the energy storage system must provide 1100 W of instantaneous peak power during eclipse, enough battery cells must be included in the design. Using a conservative battery cell number factor of safety of 1.5, SSTL's standard Sanyo 4 Ahr, 1.2 V NiCd cells, and assuming an eclipse duty cycle of 25%, one finds that the required battery capacity, C_r, in order to accomplish the mission is 164.62 Whrs. This equates to a requirement for just over 52 cells (rounded up to 55). Converting the performance for these 55 cells back to the instantaneous peak power and capacity available, P_a and C_a, yields 1667.81 W and 249.60 Whr, respectively. Then, comparing the available power and capacity to the associate required values, gives an instantaneous peak power margin of 567.81 W and capacity margin of 84.98 Whr. These are the first 2 baseline design margins. Second, the Attitude Control Subsystem, ACS, is a MW system required to do a 140 deg bang-off-bang maneuver in 70 s, with a 12 s torque dead-band. This results in a required torque of N_r for the baseline system of 0.2466 Nm. Coupling this result with a 2.6 factor increase in baseline wheel mass and radius (for a boost in inertia) yields an N_a of 1.4098 Nm, or torque margin of 1.1632 Nm. Finally, the upgraded baseline system which meets the given power and attitude control requirements checks in at 31.83 kg, with 13.17 kg below the allocated 45.0 kg.

ESACS vs. Baseline

Coupling the baseline definition with optimally sized ESACS VSCMGs and using the defined implied implementation strategy yields the Table 2 results. Here, the Alternative #3 Long-term columns reflects the desirable long-term point design based on a wheel angular acceleration of $100\,\mathrm{rad/s^2}$ and angular speed of 15300 RPM to 55200 RPM. This was found using the aforementioned realistic wheel speed range in Figure 10, which corresponds to $100\,\mathrm{rad/s^2}$. Since this design is based on equivalent performance, another way to determine this angular acceleration is to use the baseline performance margins to get the constants c_1, c_2, and c_3 and calculate $\dot{\Omega}$. Clearly, one can see this effect in reviewing the baseline capacity, power, and torque margins as compared to this design. Obviously, using an increased wheel acceleration and speed range yields an increased mass margin over the baseline with a shorter rotor length. Similarly, one enjoys a significant increase in energy and power density over the baseline system using this approach. This information is also quite valuable in assessing the effect of implementing a more conventional approach as in Alternative #1. The largest difference lying in the lifetime result. Furthermore, these results illustrate the large mass savings over the baseline in the long-term with either option. Table 3 shows a mass breakdown for these designs.

Similarly, the near-term results reflected in Tables 2 and 3 illustrate benefits which can be realized with present technology. There are definite benefits, namely energy density, power density, and lifetime, for a small satellite mission such as spotlight SAR with optimistic agility, peak power, energy storage requirements in implementing this plan, even in the short-term.

8.0 Future Work

Future work entails implementing these sizing results via laboratory experimentation. The idea is to implement currently realisable technology (i.e. Alternative #1's Near-Term results) to validate/refine the sizing approach and extrapolate a magnetic-bearing-based flywheel, ESACS VSCMG Alternative #3 system's performance. Then, as Alternative #3 becomes feasible, it can be implemented to realize increased benefits.

9.0 Conclusion

In summary, energy storage and attitude control for small satellites using VSCMGs is feasible and beneficial. Given the ESACS' wide variety of benefits, such a system can replace a conventional MW ACS plus NiCd secondary battery ES yielding greater agility, 40+% subsystem mass savings (with 3-5 % overall spacecraft mass reduction), longer lifetime for depths-of-discharge ranging from 0-80%, and increased power density (W/kg) for a given energy density (Whr/kg). In fact, one satellite mission which will thrive on these benefits is that of space RADAR.

This work reviewed the state-of-the art for a VSCMG-based ESACS. Technology trades and an analysis of three resulting alternatives was completed using a novel, nonlinear, constrained optimization-based, ESACS VSCMG actuator sizing approach presented. From it, a gimballed, magnetically-levitated, carbon fiber rotor flywheel like that of [36] best met a set of aggressive, small satellite spotlight SAR example requirements. Since this technology is not yet realisable, two three-part implementation plans (one for Alternative #3 and one for Alternative #1) were formulated to provide the most benefits from advancing technology. The next stage is to use current technology to build and test an ESACS VSCMG suite based on the near-term, Alternative #1 actuator design identified in this implementation plan. This actuator will involve a mechanically suspended, Carbon fiber rotor based on Lappas' SSTL CMG design [6], with a 3.5 cm thick rotor spinning at $15300 - 55200\,\mathrm{RPM}$ and with $66\,\mathrm{rad/s^2}$ angular acceleration. Testing this system (and thus validating the sizing and control theories) will positively advance the state-of-the-art in small satellite design, paving the way for better and cheaper agile small satellites to fulfill challenging missions previously reserved for large satellites.

10.0 Acknowledgements

The authors would like to thank Dr. Barrett Flake from the US Air Force European Office of Research and Development as well as Dr. Jerry Fausz and Dr. Brian Wilson at the United States Air Force Research Laboratory for their efforts in sponsoring this investigation. Their advice and funding support has enabled this ambitious effort to evolve.

References

[1] Ward, J., Jason, S., and Sweeting, M., "Microsatellite Constellation for Disaster Monitoring," *Proceedings of the 13th Annual AIAA/USU Conference on Small Satellites*, Logan, Utah, 1999.

[2] Bradford, A., Gomes, L., and Sweeting, M., "BILSAT-1: A Low-Cost, Agile, Earth Observation Microsatellite for Turkey," *Proceedings of the 53rd International Astronautical Congress*, Houston, Texas, October 2002.

Table 2 ESACS Development Comparison

Parameter	Base MW + NiCd	Alt #3 Long-Term	Alt #3 Mid-Term	Alt #3 Near-Term	Alt #1 Long-Term	Alt #1 Mid-Term	Alt #1 Near-Term
Wheel Acceleration, $\dot{\Omega}$, rad/s^2	25	100	80	66	100	80	66
Capacity Margin, C_m, Whr	84.98	84.98	84.98	84.98	84.98	84.98	84.98
Power Margin, P_m, W	567.8	567.8	234.25	0.754	567.8	234.25	0.754
Torque Margin, N_m, Nm	1.163	1.163	1.163	1.163	1.163	1.163	1.163
Mass Margin, M_m, kg	13.17	42.42	42.45	42.48	40.79	40.79	40.79
Wheel Speeds, $\Omega_{min} - \Omega_{max}$, RPM	0-5000	15300-55200	15300-55200	15300-55200	15300-55200	15300-55200	15300-55200
Rotor Length, l_{rot}, m	0.089	0.035	0.035	0.035	0.035	0.035	0.035
Energy Density, *Edens*, Whr/kg	7.84	121.44	123.11	124.43	74.52	74.52	74.52
Power Density, *Pdens*, W/kg	52.39	645.83	523.74	436.74	396.31	317.04	261.56
Mass Savings, *MS*, %	0.0	91.9	92.0	92.1	86.8	86.8	86.8
Lifetime, cycles	300	22000	22000	22000	505	505	505
Requirements							
Peak Power, P_r, W	1100	1100	1100	1100	1100	1100	1100
Eclipse Duty Cycle, d_{ty}, %	25	25	25	25	25	25	25

Table 3 ESACS Development Mass Breakdown

Parameter	Base MW + NiCd	Alt #3 Long-Term	Alt #3 Mid-Term	Alt #3 Near-Term	Alt #1 Long-Term	Alt #1 Mid-Term	Alt #1 Near-Term
Wheel Acceleration, $\dot{\Omega}$, rad/s^2	25	100	80	66	100	80	66
Rotor Mass, kg	1.1635	0.3060	0.3060	0.3060	0.3060	0.3060	0.3060
Motor/Generator Mass, kg	N/A	0.0827	0.0739	0.0672	0.2400	0.2400	0.2400
Magnetic Bearing or Mk II Other, kg	N/A	0.1508	0.1508	0.1508	0.4000	0.4000	0.4000
Other*, kg	3.1460	0.1061	0.1061	0.1061	0.1061	0.1061	0.1061
Mass 1 Actuator, kg	4.310	0.6456	0.6369	0.6301	1.0521	1.0521	1.0521
Total Mass, ACS plus ES or ESACS, kg	31.83	2.5824	2.5204	2.5204	4.2084	4.2084	4.2084
Spin-axis Inertia, I_{w_s}, kgm^2	0.0141	0.0010	0.0010	0.0010	0.0010	0.0010	0.0010
Rotor Dimensions							
Outer Radius, r_o, m	0.0669	0.0635	0.0635	0.0635	0.0635	0.0635	0.0635
Inner Radius, r_i, m	0.0000	0.0500	0.0500	0.0500	0.0500	0.0500	0.0500
Wheel Torque, N_w, Nm	0.3525	0.1000	0.0800	0.0660	0.1000	0.0800	0.0660
Shaft Max Power, P_s, W	184.55	576.94	461.55	380.78	576.94	461.55	380.78

* Other Mass Includes Support Structure, Electronics, Containment Vessel, Launch Lock, Baseline ES, etc.

[3]Van Der Zel, V., Blewett, M., Clark, C., and Hamill, D., "Three Generations of DC Power Systems for Experimental Small Satellites," *Proceedings of the Applied Power Electronics Conference*, Vol. 2, San Jose, CA, March 1996, pp. 664–670.

[4]Ward, J. and Sweeting, M., "First In-Orbit Results from the UOSAT-12 Minisatellite," *Proceedings of the 13th Annual AIAA/USU Conference on Small Satellites*, Logan, Utah, 1999.

[5]Richie, D., Tsiotras, P., and Fausz, J., "Simultaneous Attitude Control and Energy Storage using VSCMGs:Theory and Simulation," *Proceedings of the American Control Conference*, June 25-27 2001, pp. 3973–3979, Arlington,VA.

[6]Lappas, V., *A Control Moment Gyro (CMG) Based Attitude Control System (ACS) For Agile Small Satellites*, Phd thesis, School of Electronics and Physical Sciences, University of Surrey, Guildford, United Kingdom, October 2002.

[7]Roes, J. B., "An Electro-Mechanical Energy Storage System for Space Application," *Progress in Astronautics and Rocketry*, Vol. 3, 1961, pp. 613–622.

[8]Notti, J., Cormack, A., and Klein, W., "Integrated Power/Attitude Control System (IPACS)," *Journal of Spacecraft and Rockets*, Vol. 12, No. 8, 1975, pp. 485–491.

[9]Adams, L., "Application of isotensoid flywheels to spacecraft energy and angular momentum storage," NASA Tech. Report NASA CR-1971, Astro Research Corporation, Santa Barbara, CA, 1972.

[10]Notti, J., "Integrated Power/Attitude Control System (IPACS) Study; Vol 1 - Feasibility Studies," NASA Report CR 2383, NASA, April 1974.

[11]Anderson, W. and Keckler, C., "Integrated Power/Attitude Control System (IPACS) for Space Application," *Proceedings of the 5th IFAC Symposium on Automatic Control in Space*, 1973.

[12]Cormack III, A., "Three Axis Flywheel Energy and Control Systems," Tech. Rep. NASA TN-73-G&C-8, North American Rockwell Corp., 1973.

[13]Will, R., Keckler, C., and Jacobs, K., "Description and Simulation of an Integrated Power and Attitude Control System Concept for Space-Vehicle Application," Tech. Rep. NASA TN-D-7459, NASA, 1974.

[14]Notti, J., Schmill, W., Klein, W., and Cormack, A., I., "Integrated Power/Attitude Control System (IPACS) Study: Volume II–Conceptual Designs," Tech. Rep. NASA CR-2384, Rockwell International Space Division, Downey, CA, 1974.

[15]Kirk, J. A., "Flywheel Energy Storage Part I: Basic Concepts," *International Journal of Mechanical Sciences*, Vol. 19, No. 4, 1976, pp. 223–231.

[16]Kirk, J. A. and Studer, P., "Flywheel Energy Storage Part II: Magnetically Suspended Superflywheel," *International Journal of Mechanical Science*, Vol. 19, No. 4, 1976, pp. 233–245.

[17]"History," website: *www.hybridcars.com/history.html*, 2005, last accessed May 31, 2005.

[18]Hall, C., "High-Speed Flywheels for Integrated Energy Storage and Attitude Control," *Proceedings of the American Control Conference*, Vol. 3, June 4-6 1997, pp. 1894–1898, Albuquerque, NM.

[19]P.Tsiotras, H.Shen, and Hall, C., "Satellite Attitude Control and Power Tracking with Energy/Momentum Wheels," *AIAA Journal of Guidance, Control, and Dynamics*, Vol. 24, No. 1, 2001, pp. 23–34.

[20]Hall, C., "Integrated Spacecraft Power and Attitude Control Systems Using Flywheels," Report AFIT/ENY/TR-000, the Air Force Institute of Technology, Dayton, OH, 2000.

[21]Ford, K. A. and Hall, C. D., "Singular Direction Avoidance Steering for Control-Moment Gyros," *AIAA Journal of Guidance, Control, and Dynamics*, Vol. 23, No. 4, 2000, pp. 648–656.

[22]Ford, K. A., *Reorientations of Flexible Spacecraft Using Momentum Exchange Devices*, Ph.D. thesis, Air Force Institude of Technology, Wright-Patterson AFB, Ohio, September 1997.

[23]Schaub, H., Vadali, S. R., and Junkins, J. L., "Feedback Control Law for Variable Speed Control Moment Gyros," *Journal of the Astronautical Sciences*, Vol. 46, No. 3, 1998, pp. 307–28.

[24]Jacot, A. D. and Liska, D., "Control Moment Gyros in Attitude Control," *Journal of Spacecraft and Rockets*, Vol. 3, No. 9, 1966, pp. 1313–1320.

[25]Margulies, G. and Aubrun, J., "Geometric Theory of Single-Gimbal Control Moment Gyro Systems," *Journal of the Astronautical Sciences*, Vol. 26, No. 2, 1978, pp. 159–191.

[26]Oh, H. and Vadali, S., "Feedback Control and Steering Laws for Spacecraft Using Single Gimbal Control Moment Gyros," *Journal of the Astronautical Sciences*, Vol. 39, No. 2, 1991, pp. 183–203.

[27]Wie, B., *Space Vehicle Dynamics and Control*, American Institute of Aeronautics and Astronautics, Inc., Reston, VA, 1998, AIAA Education series.

[28]Paradiso, J., "Global Steering of Single Gimballed Control Moment Gyroscopes Using a Directed Search," *AIAA Journal of Guidance, Control, and Dynamics*, Vol. 15, No. 5, 1992, pp. 1236–1244.

[29]Bedrossian, N., Paradiso, J., Bergmann, E., and Rowell, D., "Steering Law Design for Redundant Single Gimbal Control Moment Gyroscopes," *AIAA Journal of Guidance, Control, and Dynamics*, Vol. 13, No. 6, 1990, pp. 1083–1089.

[30]Bedrossian, N., Paradiso, J., Bergmann, E., and Rowell, D., "Redundant Single Gimbal Control Moment Gyroscope Singularity Analysis," *AIAA Journal of Guidance, Control, and Dynamics*, Vol. 13, No. 6, 1990, pp. 1096–1101.

[31] Roithmayr, C., Karlgaard, C., Kumar, R., and Bose, D., "Integrated Power and Attitude Control with Spacecraft Flywheels and Control Moment Gyroscopes," *AIAA Journal of Guidance, Control, and Dynamics*, Vol. 27, No. 5, 2004, pp. 859–873.

[32] Kenny, B., Kascak, P., Jansen, R., Dever, T., and Santiago, W., "Control of a High Speed Flywheel System for Energy Storage in Space Applications," NASA TM NASA TM 2004-213356, NASA, November 2004.

[33] Kenny, B., Kascak, P., Jansen, R., and Dever, T., "A Flywheel Energy Storage System Demonstration for Space Applications," *Proceedings of the International Electric Machines and Drives Conference*, Madison, WI, June 1-4 2003, NASA TM 2003-212346.

[34] Kenny, B., Jansen, R., Kascak, P., Dever, T., and Santiago, W., "Demonstration of Single Axis Combined Attitude Control and Energy Storage Using Two Flywheels," *Proceedings of the 2004 IEEE Aerospace Conference*, Vol. 4, August 2004.

[35] Wilson, B., "Power System Design of a Spacecraft Simulator Using Energy Storage Flywheels," Power Point Presentation, April 18 2005, presentation at Aerospace Corporation's Space Power Workshop.

[36] Varatharajoo, R., *Synergisms for Spacecraft Attitude Control System*, Phd thesis, Dresden Technical University, Achen, DE, June 2003, Shaker Verlag.

[37] Schaub, H., Vadali, S. R., and Junkins, J. L., "Feedback Control Law for Variable Speed Control Moment Gyros," *Proceedings of the AAS Spaceflight Mechanics Conference*, Monterey, CA, February 1998, pp. 581–600, paper No. 98-140.

[38] Henrikson, C., Lyman, J., and Studer, P., "Magnetically Suspended Momentum Wheels for Spacecraft Stabilization," *Proceedings of the 12th AIAA Aerospace Sciences Meeting*, Washington, DC, January 30- February 1 1974, AIAA Paper No. 74-128.

[39] *Space Mission Analysis and Design*, Kluwer Academic Publishers, Boston, 3rd ed., 2003.

[40] Clark, C., *An Innovative Power System Design for an Unmanned Mission to Mars*, Ms thesis, Surrey Space Center University of Surrey, Guildford, United Kingdom, 2001.

[41] Danfelt, E., Hewes, S., and Chou, T., "Optimization of Composite Flywheel Design," *International Journal of Mechanical Sciences*, Vol. 19, No. 2, 1977, pp. 69–78.

[42] "Thick Walled Cylinders," website: *www.courses.washington.edume354a*, 2005, last accessed November 2, 2005.

[43] Bryson, A. and Ho, Y., *Applied Optimal Control: Optimization, Estimation, and Control*, Hemisphere Publishing Corporation, revised printing ed., 1975.

[44] Song, Y., *Motion Compensation of Spotlight SAR Images in the Presence of Unknown Translational Target Motion*, Ms thesis, Department of Electrical and Computer Engineering, Queen's University, Kingston, Ontario, Canada, March 1998.

Science & Technology Satellites

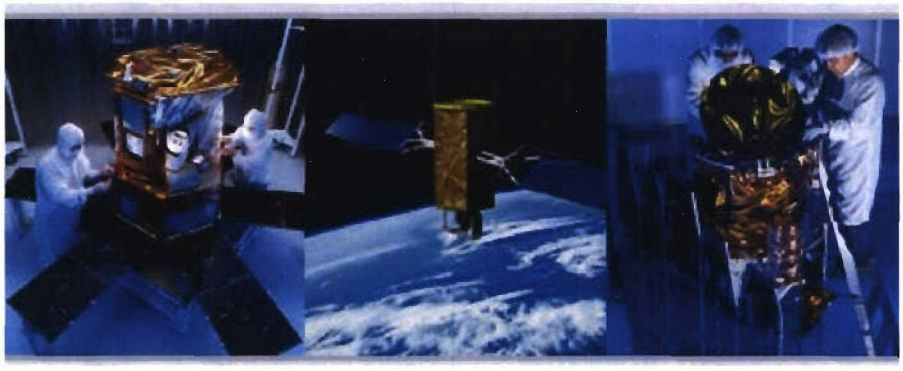

Orbital is one of the industry's leading providers of low Earth orbit (LEO) satellites. Over the past two decades, Orbital has delivered nearly 100 small satellites that have performed national security, commercial communications, Earth and space science, remote imaging and technology demonstration missions. Orbital is currently under contract to deliver another 12 satellites over the next four years. Our flight-proven spacecraft can support a variety of payloads and are highly reliable, having amassed nearly 450 years of in-orbit experience. Our LEO spacecraft serve four primary markets:

Earth and Space Science

Working hand-in-hand with Principal Investigators and NASA, we have developed affordable and reliable spacecraft busses designed to support a variety of Earth and space science payloads and missions. Current LEO programs include the NASA-funded Aeronomy of Ice in the Mesosphere (AIM), Orbiting Carbon Observatory (OCO), Interstellar Boundary Explorer (IBEX), and Glory missions. Recent programs have included the Galaxy Evolution Explorer (GALEX), Solar Radiation and Climate Experiment (SORCE), the Active Cavity Radiometer Irradiance Monitor (ACRIMSAT), and Far Ultraviolet Spectroscopic Explorer (FUSE).

Remote Sensing

In the mid-1990's, we helped to establish the commercial remote sensing market with the development and launch of the OrbView series of satellites. OrbView-1 helped scientists to study lightning patterns and to collect data on dangerous weather systems. OrbView-2 was the first commercial satellite to supply daily imagery of the Earth. It has enabled researchers to better monitor the health of oceans and land vegetation and has allowed fisherman to more efficiently locate schools of tuna. The OrbView-3 high-resolution imaging satellite provides imagery for commercial, environmental and national security applications.

Web Results

Page 1 of 7,091 results containing **Attitude control subsystem for small satellites** (1.32 seconds)

Magnetic Torquers for Spacecraft **Attitude Control**

solutions for Space projects from **small**, low-cost single **satellites** to large-scale constellations. • Torquer engineering and **attitude control subsystem** design
www.smad.com/analysis/torquers.pdf Cached page PDF file

DSCS-3 Military Communications Satellite

... with increased radiated power for users with **small** ... terminals and to permit AJ communications and **satellites** ... **Attitude Control Subsystem** (ACS). The ACS is a three-axis, zero momentum ...
www.fas.org/spp/military/program/com/dscs_3.htm Cached page

Bristol Aerospace - Defence and Space

Small Satellites Bristol has been selected by the Canadian Space Agency to build the ... these include th and Data Handling (C&DH) Unit, the **Attitude Control** System (ACS), the Power **Subsystem** ...
www.bristol.ca/SmallSatellites.html Cached page

AeroAstro's Spacecraft **Subsystem** and Component Products

... and non-AeroAstro **satellites** for coarse and fine **attitude** sensing ... ideal for the needs of many **smal** being ... in concert, with the **attitude control** ...
www.aeroastro.com/products/components/products_attitude-d.php Cached page

AeroAstro's Spacecraft **Subsystem** and Component Products

... MicroCore Avionics Module serves the needs of **small** satellite ... Power **Control**, Power Switchin and Power PC 750 ... Avionics Module include university **satellites** ...
www.aeroastro.com/products/components/products_avionics.php Cached page 4/2/2006

Show more results from "www.aeroastro.com".

What Is a Satellite?

Some **satellites** are natural, like the moon, which is ... TV is a system for receiving television using a ver **attitude control subsystem** maintains the communications ...
www.boeing.com/defense-space/space/bss/sat101.html Cached page 4/4/2006

MR SAT: Missouri-Rolla Satellite Project: **Attitude** Determination and ...

... thermal properties of each material used on the **satellites** has been made. Batteries have a very **smal** **Subsystem**: **Attitude** Determination and **Control** Communications Launch Vehicle Onboard ...
web.umr.edu/~mrsat/thermal.html Cached page

Spacecraft » **Attitude** Dynamics & **Control**

Small changes in process may be made without much concern or documentation, until the **subsystem** fa or test. ... system includes three reaction wheels for **attitude control** ...
krishl.us/spacecraft/?cat=4 Cached page

Formation Flying Demonstration Missions Enabled by CanX Nanosatellite ...

Conference on **Small Satellites** 1 Formation Flying ... to the otherwise passive thermal **control subsyst** communicate with both **satellites**. The **attitude** determination and **control** ...
www.utias-sfl.net/docs/canx245-ssc-2005.pdf Cached page PDF file 4/4/2006

Web Desktop News Images Local (BETA) Encarta

small satellites and earth imaging Search

+Search Builder Settings Help Español

Web Results

Page 1 of 78,808 results containing **small satellites and earth imaging** (0.31 seconds)

earth satellites - www.ewoss.com SPC

Your Search Ends Here. We Found It: earth satellites

Science & Technology **Satellites**

Over the past two decades, Orbital has delivered nearly 100 **small satellites** that have performed nation commercial communications, **Earth** and space science, remote **imaging** and technology ...

www.orbital.com/SatellitesSpace/LEO/index.html Cached page

Images of Saturn and All Available **Satellites**

Target is Saturn (and available **satellites**) To see images of just one ... **Imaging** Science Subsystem - Na 770x440x1 PIA08147: ... **Small** Moons on the Edge Full Resolution ...

photojournal.jpl.nasa.gov/targetFamily/Saturn Cached page 4/4/2006

Images of Mars and All Available **Satellites**

Target is Mars (and available **satellites**) To see images of just one ... Thermal Emission **Imaging** Sy 1369x2978x1 PIA08026: Dunes ... **Small**, Bouldery Crater Full Resolution ...

photojournal.jpl.nasa.gov/targetFamily/Mars Cached page 4/3/2006

Show more results from "photojournal.jpl.nasa.gov".

Wired News: A Big Leap for **Small Satellites**

... pave the way for a future in which every country would have its own fleet of smart, **small satellites**. ... in cooperating with Europe on satellite technologies, particularly **Earth-imaging** ...

www.wired.com/news/technology/0,1282,60611,00.html Cached page

Satellites to study **Earth**'s magnetosphere in the future

... out as 10 times the diameter of the **Earth**. This way, scientists can measure **small** ... feature three unc "non-**imaging** ... Scientists use virtual **satellites** to explore **Earth**'s magnetosphere ...

science.nasa.gov/newhome/headlines/ast30oct98_1.htm Cached page

AeroAstro's Publications

Cohen, Gloyer, Rogan – 16th Annual AIAA/USU Conference on **Small Satellites** – 2002] Download PDF NanoObservatory™: **Earth Imaging** for Everyone

www.aeroastro.com/publications.php Cached page

Indian **Small** EO **Satellites** To Study Atmosphere

... series of dedicated **small** satellite missions to study the **earth**'s ... the new proposal called the **Small S** Indian **Small** EO **Satellites** To Study Atmosphere Space **Imaging** Awarded Additional $24 ...

www.spacemart.com/reports/Indian_Small_EO_Satellites_To_Study_Atmosphere.html Cached page

Small Satellites May Play Big Role In Future Interplanetary Missions

Proponents of **small satellites** say that tiny spacecraft have potentially ... several hundred kilograms—ar largely to low **Earth** ... and would circle the planet at a lower altitude, **imaging** the ...

space.com/spacenews/businessmonday_050808.html Cached page

JINSA Online -- Commercial Spy **Satellites** Challenge Pentagon Planners

Web Results

Page 1 of 270,665 results containing **SAR mission** (0.45 seconds)

Search & Rescue Info: **SAR**-Related Links

SAR Mission Report Form University of Alberta **SAR** Magazines Advanced Rescue Technology Magazir First Responders & Rescuers Search & Rescue Magazine California, USA

www.sarinfo.bc.ca/Sarlinks.htm Cached page

Search & Rescue Info - Tech Tips!

SAR Mission Report Form NASAR's web-based **Mission** Report Form **SAR** Post-**Mission** Reviews Benefits of **SAR** Reviews - by Martin Colwell Search Priority An Integrated Approach to Search Plani

www.sarinfo.bc.ca/Sartechs.htm Cached page 4/4/2006

Show more results from "www.sarinfo.bc.ca".

SAR Technology Inc. - Home Page

of your **mission**! **SAR** Technology announces the release of ' Incident Commander 5.0 ... Manages Sear Emergency-Response missions! - Familiar ICS structure for ...

www.sartechnology.ca Cached page 4/3/2006

Search Manager V3 - Example **Mission**

sartechnology.ca/sartechnology/SearchManagerV3_ExampleMission_viewlet_swf.html Cached page

NASA GSFC Search and Rescue **Mission** Office

Search and Rescue (**SAR**) **Mission** Manager + View Bio James E. Mentall, **SAR Mission** Deputy Manag James W. Christo , **SAR Mission** Ground Systems Manager

searchandrescue.gsfc.nasa.gov Cached page 4/4/2006

lsespace.com [TERRA **SAR Mission**]

The TerraSAR **mission** has its origin in an industrial initiative to provide market-derived X- and L-band **S**, from a pair of spacecraft operating in tandem in a sun-synchronous orbit

www.lsespace.com/missions/terrasar.php Cached page

lsespace.com [**SAR** LUPE **Mission**]

Mission and System The **SAR**-Lupe System consists of 5 identical satellites, which will be launched 6 months. It serves the German Federal Armed Forces as a national ...

www.lsespace.com/missions/sarlupe.php Cached page

Show more results from "www.lsespace.com".

SAR- Mission

setting out the **mission** of **SAR** ... President's Message Who We Are Native American Fellowships Cathe

www.sarweb.org/home/mission.htm Cached page

U.S. Coast Guard Search and Rescue

Information source for the U.S. Coast Guard's Search and Rescue (**SAR**) program. Includes points of cor Rescue Coordination Centers, **SAR** statistics, links to other **SAR** resources, the ...

www.uscg.mil/hq/g-o/g-opr/sar.htm Cached page

The X-**SAR** User Kit

Welcome to the X-**SAR** User Kit! Edited by Michael Eineder and Hartmut Runge (c) DLR/DFD, all rights r

Web Results

Page 1 of 1,479 results containing **sizing actuators for small satellite applications** (0.66 seconds)

Actuators in Action

We offer a complete line of linear **actuators** and accessories to ... **Applications** vary from processing mi rooms, automated ... They are used to open, close or position **satellite** antennas ...
www.tksimplex.com/html/actuators_in_action.html Cached page

Electronic Projects

The **satellite actuators** can draw upwards of 15 Amps ... One of these **applications** is a **small** lighting h good judgement when **sizing** the power MOSFETs for higher power **applications**.
www.redrok.com/electron.htm Cached page

C-Band Books

... link analysis, adjacent **satellite** interference and dish **sizing** ... and terrestrial mobile **applications** and methods **Satellite** ... and III is available at a **small** additional cost. DISH **SIZING** ...
66.225.242.100/cyberstore/Cband/Books.htm Cached page

Army FY04.3 SBIR Solicitation Topics

A04-054 Miniature **Actuators** for **Small** Arms ... Superconductor Technology for SATCOM **App** 134 Multi-Band **Satellite** Terminal Feed ...
www.acq.osd.mil/sadbu/sbir/solicitations/sbir043/army043.htm Cached page

Boating & Marine Supply Blog | Outdoor Marine

... so all you have to do is find the antenna for the **applications**. ... reinforced stainless steel and powerfu hydraulic **actuators**. ... Marine **Satellite** Radios Marine Antennas Reviews will include:
blog.outdoor-marine.com Cached page

ATI

Back-of-the envelope equations for actuator **sizing** ... and protocols; regulatory bodies; **satellite** services **applications**; steps ... Designing the **small satellite** power system. 7. Spacecraft ...
www.aticourses.com/Vol_82H.pdf Cached page PDF file

Titles available from 2001

Microelectromechanical Systems (MEMS) **Actuators** for ... Preliminary **Sizing** of Vertical Take-Off Rocke Communications for Aeronautics **Applications**-Technology Development and Demonstration
gltrs.grc.nasa.gov/cgi-bin/gltrs/browse.pl?2001 Cached page 4/2/2006

Creative Career Systems

... contract and tool records, handling rush orders, the **small** ... special duct problems and duct maintenar **sizing**, air ... television, how **satellite** television works, popular **applications** for **satellite** ...
www.creative.on.ca/courses/industrial.htm Cached page

DARPA SBIR 2003

... system completely integrated: sensors and **actuators** ... as well as tools to predict routing **sizing** ... ma interferences, as is required for **small satellite applications**.
www.darpa.mil/sbir/20032SBIRAwards.html Cached page

LabTrader Scientific Equipment, autoclave, centrifuge, hplc, fermentor ...